Journal of Sound and Vibration (2000) **233**(2), 297–310
doi:10.1006/jsvi.1999.2802, available online at http://www.idealibrary.com on IDEAL®

NON-LINEAR VIBRATION OF A TORSIONAL SYSTEM DRIVEN BY A HOOKE'S JOINT

S. F. ASOKANTHAN AND P. A. MEEHAN†

Department of Mechanical Engineering, The University of Queensland, Brisbane, Qld. 4072, *Australia*

(*Received* 4 *December* 1995, *and in final form* 22 *November* 1999)

Non-linear vibration in a driveline which incorporates a Hooke's joint is presented in this paper. In particular, torsional vibration due to fluctuating angular velocity ratio across the joint is examined. Linearized equations are used for the prediction of critical speed ranges where parametric instabilities characterized by exponential build up of torsional response amplitudes occur. Predicted instabilities indicate the range of driveshaft speeds to be avoided during the design of a driveline which employs a Hooke's joint. Numerical simulations and bifurcation analysis performed on the full non-linear equations further demonstrate the existence of parametric, quasi-periodic and chaotic motion. Onset of chaotic motion was shown to be characterized by a quasi-periodic route.

1. INTRODUCTION

A driveline connected by a Hooke's joint may exhibit severe twisting motion primarily due to fluctuating angular velocity ratio inherent in such systems. This motion causes noticeable noise, severe mechanical shakings, and premature fatigue failures in shafts, dog clutches, gear teeth, etc. The occurrence as well as severity of these detrimental torsional vibrations depend on the range of engine or drive shaft speeds. Torsional vibration caused by the presence of a Hooke's joint in a power transmission driveline is investigated in this paper. For this purpose, a linear as well as a complete non-linear analysis are employed. The primary intent of this study is to examine instabilities as well as chaotic response resulting from the inherent non-linearities of the system under consideration.

Porter [1] investigated this problem considering a linearized one-degree-of-freedom model and predicted the critical speed ranges. His investigation was also concerned with the effects of parameters such as stiffness ratio and joint angle on the critical speed ranges. This analysis was later extended by Porter and Gregory [2] to a non-linear model in order that the resulting amplitudes of unstable oscillation may be predicted. Subsequently, Porter [3] investigated this problem by considering a two-degree-of-freedom model and established both the instability conditions as well as the amplitudes of the steady state motion. However, the occurrence of combination resonances, the corresponding input shaft speed ranges and conditions for instabilities were not predicted in the above studies. Recently, Asokanthan and Hwang [4] employed the method of averaging and established closed-form instability conditions associated with combination resonance. However, in the above study, only the linearized equations were considered, and as a result critical speed

†Now at Industrial Automation Services, Newcastle, Australia.

0022-460X/00/220297 + 14 $35.00/0

ranges due to quasi-periodic and chaotic motion were not predicted. In the present study, critical speed ranges which correspond to the sub-harmonic and combination resonance predicted by the linear analysis are first confirmed using numerical simulation of the full non-linear equations. In addition, the existence of speed ranges due to quasi-periodic and chaotic motion is established. It is also shown that the resulting route to chaos is via a quasi-periodic route.

The governing equations representing the torsional motion of the rotor system are stated first, taking into account the well-known Hooke's joint kinematics, the flexibility of drive shafts, and the viscous damping associated with the rotation of drive shafts. These equations, when suitably linearized, represent the motion of a dynamical system with periodically varying stiffness and inertia. The method of averaging is used for obtaining conditions for onset of instabilities in the neighbourhood of certain multiples and combination of system natural frequencies. Numerical simulations were carried out on the full non-linear equations and critical speeds were predicted using typical indicators such as Lyapunov exponents, power spectrum and poincare maps. These predictions are also confirmed via bifurcation analyses performed with respect to the joint angles as well as running speeds.

2. EQUATIONS OF MOTION

For the purposes of the present analysis, a two-degree-of-freedom system incorporating a Hooke's joint as illustrated in Figure 1 is considered. This rotational system having an angular misalignment of θ is driven at a constant angular velocity Ω. The quantities α_1, β represent the input and the output angles of the Hooke's joint, respectively, while α_2 symbolizes the output angle of the system. The input and the output shafts have been considered to be flexible and to have torsional stiffnesses S_1, S_2 respectively. The moments of inertia associated with the input and output drive systems are denoted by I_1 and I_2, respectively, which also takes the driven inertia load into consideration. It is also assumed that both input as well as output shafts of the system are massless and their flexural vibrations are considered to be completely prevented by the associated support bearings. The energy dissipation associated with the rotational motion of I_1 and I_2 are taken to be proportional to the viscous damping coefficients C_1 and C_2 respectively.

Equations of motion in terms of the twist variables x and y may be derived using Lagrange's equations (see e.g., references [1, 4]). The twist variables x and y are represented

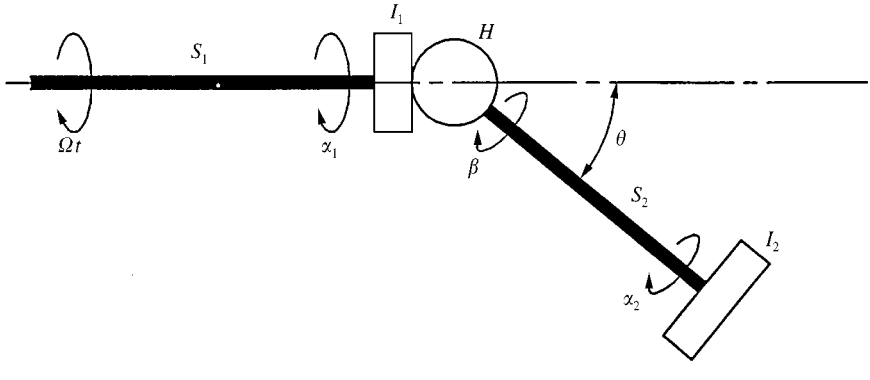

Figure 1. Driveline incorporating a Hooke's joint.

by $\alpha_1 - \Omega t$ and $\alpha_2 - \beta$ respectively. In deriving the equations, the linearized form of the well-known kinematic relationship between the input and output angular velocities across a Hooke's joints has been employed. The resulting equations are

$$\ddot{x} + \omega_{11}^2 x - \omega_{21}^2 y = \varepsilon\left\{\frac{\omega_{21}^2 y\cos(2x + 2\Omega t)}{2} - 2\mu_{11}\omega_{11}(\dot{x} + \Omega)\right\} + O(\varepsilon^2),$$

$$\ddot{x}+\ddot{y}+\omega_{22}^2 y=\varepsilon\left\{(\dot{x}+\Omega)^2\sin(2x+2\Omega t) - \frac{\ddot{x}\cos(2x + 2\Omega t)}{2} - 2\mu_{22}\omega_{22}(\dot{x} + \dot{y} + \Omega)\right\} + O(\varepsilon^2). \tag{1}$$

In the above equations,

$$\omega_{11}^2 = S_1/I_1, \quad \omega_{21}^2 = S_2/I_1, \quad \omega_{22}^2 = S_2/I_2, \quad C_1/I_1 = 2\varepsilon\mu_{11}\omega_{11}, \quad C_2/I_2 = 2\varepsilon\mu_{22}\omega_{22},$$

$$\varepsilon = \sin^2\theta,$$

where $O(\varepsilon^2)$ represents the smaller terms of order ε^2 or higher.

Equations (1) represent the torsional motion of the two-degree-of-freedom system incroporating a Hooke's joint and contain periodically varying coefficients. These coefficients are seen to be non-linear functions of the state variables. It is known that closed-form solutions to these equations are not available, but, insight into the instability behaviour may be obtained by considering the linearized equations. Equations (1) are analyzed numerically in a subsequent section. In the sequel, a stability analysis is performed by considering the linearized system.

3. LINEAR ANALYSIS USING THE METHOD OF AVERAGING

In order to examine the stability behaviour of the solution corresponding to the equilibrium configuration, the equations of motion are linearized and the resulting equations with non-homogeneous terms deleted are examined for stability of their solution. The linearized equations are

$$\ddot{x} + \omega_{11}^2 x - \omega_{21}^2 - \omega_{21}^2 y = \varepsilon\left\{\frac{\omega_{21}^2}{2} y\cos(2\Omega t) - 2\mu_{11}\omega_{11}\dot{x}\right\},$$

$$\ddot{x} + \ddot{y} + \omega_{22}^2 y = \varepsilon\left\{2\Omega^2 x\cos(2\Omega t) - 2\mu_{22}\omega_{22}(\dot{x} + \dot{y}) + 2\Omega\dot{x}\sin(2\Omega t) - \frac{\ddot{x}\cos(2\Omega t)}{2}\right\} \tag{2}$$

which contain periodic coefficients of frequency 2Ω.

Before performing a stability analysis, it is first necessary to evaluate the natural frequencies of the torsional modes in terms of other system parameters. For this purpose, homogeneous equations (2) are reduced by setting the misalignment parameter ε to zero to obtain the following equations:

$$\ddot{x} + \omega_{11}^2 x - \rho\omega_{11}^2 y = 0, \qquad \ddot{x} + \ddot{y} + \omega_{22}^2 y = 0. \tag{3}$$

In equations (3), the quantity ρ represents the stiffness ratio S_2/S_1. The natural frequencies can be evaluated to be

$$\omega_{1,2}^2 = \tfrac{1}{2}(\omega_{11}^2 + \omega_{22}^2 + \rho\omega_{11}^2 \mp \sqrt{(\omega_{11}^2 + \omega_{22}^2 + \rho\omega_{11}^2)^2 - 4\omega_{11}^2\omega_{22}^2}). \tag{4}$$

In expression (4), the upper sign refers to ω_1^2 while the lower sign refers to ω_2^2.

It may be seen from equations (4) that the natural frequencies ω_1, ω_2 are always real for any set of system parameter values and hence equations (2) represent the free motion of a linear non-gyroscopic system. It is known that exact solutions, in a closed form, to the governing equations (2) are not available. However, an asymptotic method such as the method of averaging (see e.g., reference [5]) may be used to obtain an approximate solution. This method has been successfully applied to gyroscopic systems which represented moving elastic bands and chain drives (see, e.g., references [6, 7]). The method of averaging has also been successfully employed for examining the stability of the present system governed by equation (1). Complete description of the method and the analysis have been presented by Asokanthan and Hwang [4]. The main results are summarized in the present paper.

It has been shown that parametric instabilities characterized by exponential build up of amplitudes will occur when the excitation frequency 2Ω is in the neighbourhood of certain multiples and combinations of the natural frequencies, ω_1 and ω_2.

3.1. SUB-HARMONIC RESONANCE

In this case, the onset of instability occurs if the excitation frequency 2Ω lies in the neighbourhood of $2\omega_p$, $p = 1, 2$. Under this condition, Asokanthan and Hwang [4] obtained the following closed-form expression for the stability condition:

$$\omega_p = [1 - 2\sqrt{\varepsilon^2\eta_p^2 - (\varepsilon\chi_p)^2}] < \Omega < \omega_p[1 + 2\sqrt{\varepsilon^2\eta_p^2 - (\varepsilon\chi_p)^2}], \tag{5}$$

where

$$\eta_p = \frac{1 - 2\rho\lambda_p - \rho\lambda_p\lambda_s}{16(\lambda_p - \lambda_s)(1 - \rho\lambda_p)}, \quad p = 1, 2,$$

$$\lambda_p = \frac{\omega_{11}^2 - \omega_p^2}{\rho\omega_{11}^2} = \frac{\omega_p^2}{\omega_{22}^2 - \omega_p^2} \quad p = 1, 2,$$

$$\varepsilon\chi_p = \frac{(C_1/I_1)(1 + \lambda_s) - (C_2/I_2)(1 + \lambda_p)}{4\omega_p(\lambda_p - \lambda_s)}, \quad p, s = 1, 2,\ p \neq s.$$

When the damping constants C_1, C_2 are negligible, the instability condition (5) reduces to

$$\omega_p[1 - 2\eta_p\varepsilon] < \Omega < \omega_p[1 + 2\eta_p\varepsilon]. \tag{6}$$

3.2. COMBINATION RESONANCE

In this case, instabilities are initiated via combination resonance which takes place when the frequency of excitation 2Ω lies in the neighbourhood of sum or difference of the natural frequencies (i.e., when $\Omega \approx |\omega_p \pm \omega_s|$, $p, s = 1, 2$, $p \neq s$). The stability condition in this case of additive combination resonance can be shown to take the form

$$(\omega_1+\omega_2)\left\{\frac{1}{2} - \frac{1}{2}\left(r + \frac{1}{r}\right)\varepsilon\sqrt{\eta_3\eta_4 - G_1G_2}\right\} < \Omega < (\omega_1+\omega_2)\left\{\frac{1}{2} + \frac{1}{2}\left(r + \frac{1}{r}\right)\varepsilon\sqrt{\eta_3\eta_4 - G_1G_2}\right\}, \tag{7}$$

where

$$G_p = \left[\mu_{11} \frac{1+\lambda_s}{\sqrt{1-\rho\lambda_p}} - \mu_{22} \frac{(1+\lambda_p)^{3/2}}{\sqrt{\lambda_p}} \right] \frac{\omega_p}{\omega_p + \omega_s}, \quad p, s = 1, 2,\ p \neq s$$

and $r = \sqrt{G_1/G_2}$ while η_3 and η_4 are given by the following expressions:

$$\eta_3 = \frac{\omega_1}{\omega_1 + \omega_2} \left\{ \frac{1}{8(\lambda_1 - \lambda_2)} \left(1 - \frac{(1+\lambda_2)\lambda_2}{\omega_1^2} \frac{S_2}{I_1} \right) \right\},$$

$$\eta_4 = \frac{\omega_2}{\omega_1 + \omega_2} \left\{ \frac{1}{8(\lambda_1 - \lambda_2)} \left(\frac{(+\lambda_1)\lambda_1}{\omega_2^2} \frac{S_2}{I_1} - 1 \right) \right\}.$$

In the absence of damping, condition (7) reduces to

$$(\omega_1 + \omega_2)\{\tfrac{1}{2} - \varepsilon\sqrt{\eta_3\eta_4}\} < \Omega < (\omega_1 + \omega_2)\{\tfrac{1}{2} + \tfrac{1}{2}\varepsilon\sqrt{\eta_3\eta_4}\}. \tag{8}$$

It may be noted that unlike in the sub-harmonic case, in this form of instability, both modes participate simultaneously. It may also be deduced from the instability conditions that if the damping constants C_1 and C_2 do not satisfy the condition $r = 1$, then the unstable speed range becomes wider than the corresponding range for the undamped case. In the case of combination resonance of the difference type, i.e., when the excitation frequency 2Ω is in the neighbourhood of $\omega_1 - \omega_2$, it has been shown that the system is always stable.

In order to predict all possible critical speed ranges and the associated response amplitudes, the linear analysis is not adequate and a non-linear analysis is required. In addition, a non-linear analysis will identify other unstable behaviour resulting from non-linearities. It will also serve to confirm the results obtained using the linear analysis. To this end, since an analytical analysis is cumbersome, it is expedient to resort to a numerical investigation.

4. NON-LINEAR ANALYSIS

Equations of motion (1) are used for the non-linear analysis of the system. For the purpose of numerical simulations they are rearranged into the following state variable form:

$$\dot{X}_1 = X_2, \qquad \dot{X}_2 = \alpha(X)\varepsilon - \beta(X), \qquad \dot{X}_3 = X_4,$$

$$\dot{X}_4 = \varepsilon\chi(X) - \dot{X}_2(\varepsilon\phi(X, t) + 1) - \omega_{22}^2 X_3, \qquad \dot{X}_5 = \Omega, \tag{9}$$

where $[X_1\ X_2\ X_3\ X_4\ X_5] = [x\ \dot{x}\ y\ \dot{y}\ \Omega t]$ and

$$\phi(X, t) = \tfrac{1}{2}\cos(2X_1 + 2X_5), \qquad \alpha(X) = \omega_{21}^2 \phi(X, t) X_3 - 2\mu_{11}\omega_{11}(X_2 + \Omega),$$

$$\beta(X) = \omega_{11}^2 X_1 - \omega_{21}^2 X_3, \qquad \chi(X) = \sin(2X_1 + 2X_5)(X_2 + \Omega)^2 - 2\mu_{22}\omega_{22}(\Omega + X_2 + X_4),$$

This set of first order non-linear state equations of motion was used to investigate the non-linear dynamical behaviour of the driveline via numerical integration. The details of the method of integration and the results are presented in the following section.

5. NUMERICAL RESULTS AND DISCUSSION

In order to illustrate the applicability of the analytical results presented in the previous sections, an experimental driveline that has been developed at the University of Queensland is considered. The parameters chosen for the present study conform to the above experimental system. The values selected for torsional stiffness, moment of inertia and viscous damping coefficient for each shaft were $S_1 = 25$ Nm, $S_2 = 250$ Nm, $I_1 = 0{\cdot}042$ kg m^2, $I_2 = 0{\cdot}084$ kg m^2, $C_1 = 0{\cdot}04$ Nm s and $C_2 = 0{\cdot}18$ Nm s respectively. The damping constants associated with the first and second modes were selected to be 2% of critical damping. For these parameters, the natural frequencies ω_1, ω_2 associated with the torsional vibration in the first and second modes take the values 13·78 and 96·61 rad/s respectively. In this case, the primary combination resonance frequency ω_c takes the value of 55·19 rad/s. All numerical integrations began from the initial conditions described by $[x\ \dot{x}\ y\ \dot{y}\ \Omega t] = [0\ 0\ 0\ 0\ 0]$ which is physically representative of the shafts under steady rotation and no twist.

5.1. CRITICAL SPEEDS PREDICTED VIA LINEAR ANALYSIS

Figure 2 shows the instability regions for the above system parameter values plotted in the excitation parameter-input shaft speed space using equations (6) and (8). The straight lines attached to each region represent the stability boundaries associated with the undamped systems. The first and the third regions shown in this figure correspond to the sub-harmonic resonances while the middle region corresponds to the combination resonance of the additive type. It may be recalled here that the excitation parameter ε is equal to $\sin^2\theta$, θ being the Hooke's joint angle. It may be seen from this figure that the regions become wider with increasing joint angle. It can be shown that these regions become narrower and become elevated in the parameter space if damping is taken into account via equations (5) and (7). It is worth noting that the region for the additive-type combination

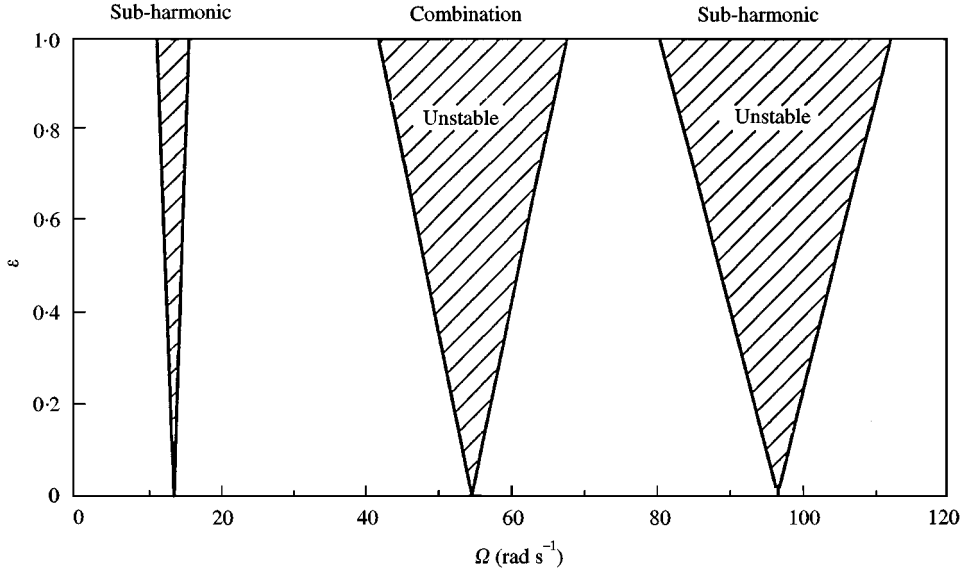

Figure 2. Instability regions predicted by linear analysis.

resonance was identified for the first time in a Hooke's joint drive system by Asokanthan and Hwang [4].

5.2. CRITICAL SPEEDS PREDICTED VIA NON-LINEAR ANALYSIS

The non-linear dynamical behaviour of the driveline was then investigated numerically by integrating the non-linear state-space equations of motion (9). All numerical simulations were performed on a Sun SPARC Station IPX using DSTOOL, written by Guckenheimer and DYNAMICS, written by Nusse and Yorke [8]. The fourth order Runge–Kutta routine was used for numerical integration. Various tools such as Poincare maps, fast fourier transform (FFT), Lyapunov spectrum, Lyapunov dimension and bifurcation diagrams of time history and largest Lyapunov exponents were used to examine the non-linear phenomena. All of the above indicators were obtained using DYNAMICS except the FFT which was calculated within the MATLAB environment. The Lyapunov exponents were calculated using the algorithm derived by Wolf *et al.* [9] and iterated at least 5000 periods of the input angular velocity Ω to within 0.5% error. Renormalization was performed at a frequency of 80 Ω. The Lyapunov spectrum and dimension were calculated to within 0.1 and 0.02% error respectively. At least 45 forcing periods were considered when using the FFT for generating power spectra. In what follows, instabilities were identified and characterized for the cases of varying input speed and varying Hooke's joint angle.

5.2.1. *Case I*: *Predictions for input speed variation*

The characteristic non-linear phenomena were investigated initially by varying the amplitude of the input angular velocity. Figure 3(a) provides useful information on the time history of the system as the input angular velocity is varied from $\Omega = 5$ to 120 rad/s for a Hooke's joint angle of 40°. This figure depicts the extreme values of the twist of the output shaft, y, for a range of input angular velocity, Ω, after transient conditions have subsided. Instability regions may be identified in the figure as large increases in amplitude of twist. Note that bounded motion is still present in the instability regions due to the non-linearities within the system. As illustrated, criteria for the onset of parametric subharmonic resonance can be identified for both natural frequencies in the form $2\Omega = 2\omega_p/n$; $p = 1, 2$ for $n = 1, 2, 4, 6. 8$. These critical speeds which correspond to the primary resonances are the same as those predicted by the approximate linear analysis. In addition, a number of combination resonances in the general form of $2\Omega = l\omega_p \pm m\omega_s/n$; $p = 1, 2$, $p \neq s$, l, m, n being positive integers, may be identified from this figure. Note that the resonant behaviour seen at $\Omega \approx 63$ and 106 rad/s were not predicted by the linear analysis and are the result of non-linearities within the system. Other forms of this general combination resonance were found to appear as the Hooke's joint angle was increased further. The variation of the maximal Lyapunov exponent as the Hooke's joint angle was increased further. The variation of the maximal Lyapunov exponent as the input speed is varied for the same set of parameters is depicted in Figure 3(b). From this figure it is evident that the parametric resonance phenomena described above are indicated by a sudden increase in the maximum Lyapunov exponent of the system. Note that the exponent may not become positive near resonance speeds as the resulting motion is non-transient and bounded due to the non-linearities in the system. In fact, the present deterministic system has a positive maximum Lyapunov exponent only when the corresponding motion of the system is chaotic. A zero maximum Lyapunov exponent indicates quasi-periodic motion which is non-periodic motion arising from the combination of two or more distinct frequencies. As illustrated in Figure 3(b), quasi-periodic motion occurs near $\Omega \approx 28{,}52{,}63{,}106$ and 111 rad/s which are the

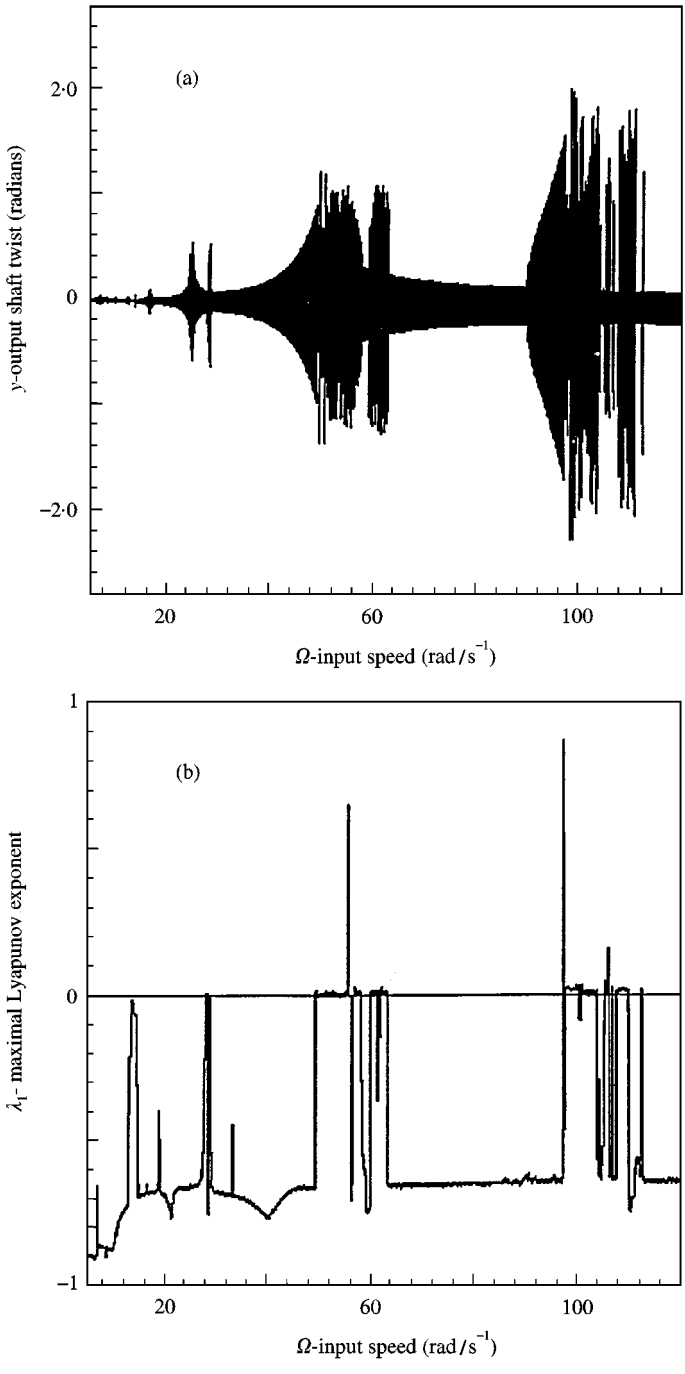

Figure 3. Variation of (a) extreme values of steady state twise, (b) maximal Lyapunov exponent: $\theta = 40^\circ$ and ω range of 5–120 rad/s.

combination resonance frequencies. At these input shaft speeds the motion of the output shaft is a result of incommensurate combinations of the natural frequencies ω_1 and ω_2. Chaotic motion, indicated by a positive maximum Lyapunov exponent, is seen to occur at $\Omega \approx 56{,}97{\cdot}4, 106$ rad/s.

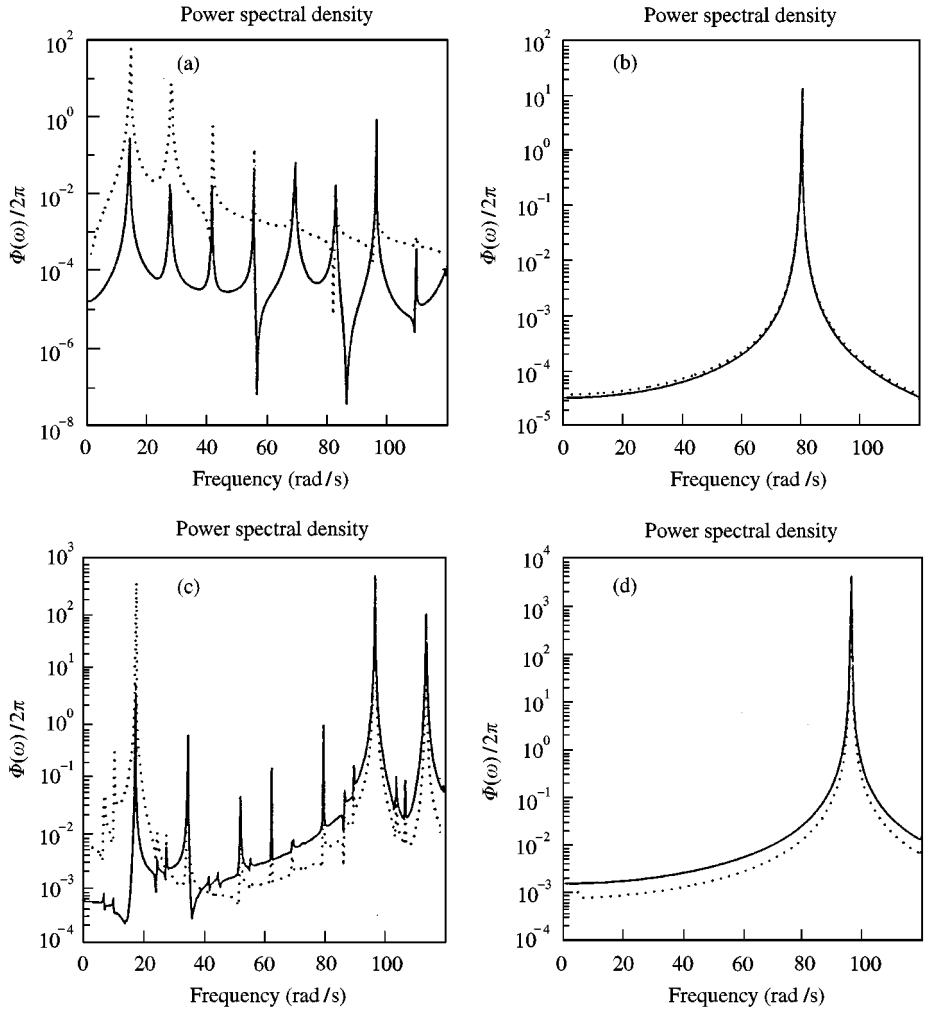

Figure 4. Powder spectral density for $\theta = 40°$. (a) $\Omega = 13{\cdot}7$ rad/s; (b) $\Omega = 40$ rad/s; (c) $\Omega = 55{\cdot}2$ rad/s; (d) $\Omega = 96{\cdot}6$ rad/s.

Figure 4 describes the power spectral density of the system for the same parameters at four different input shaft speeds $\Omega \approx 13{\cdot}7, 40, 55{\cdot}2, 96{\cdot}6$ rad/s. Parametric instability is evident when the input speed is close to each natural frequency $\omega_1 = 13{\cdot}7$ rad/s, and $\omega_2 = 96{\cdot}6$ rad/s, as indicated in Figures 4(a) and 4(d), since the output motion frequency is the same as a natural frequency in both cases. For the stable case depicted in Figure 4(b), when the input speed is at 40 rad/s, we notice that the output frequency is at double the input speed Ω due to the forced excitation resulting from the Hooke's joint angle as seen in equations (1) and (2). This was the case for all stable speeds. The combination resonance condition is indicated in Figure 4(c) for an input speed of 55.2 rad/s. The frequency spectrum in this case indicates that the resulting motion is made up of a combination of frequencies in the form $\Omega = n\omega_1 \pm m\omega_2$ where n, m are integers starting from 0. The presence of these mixing components in the spectrum indicates that the time-dependent processes are strongly non-linear. These frequencies are incommensurate as the maximum Lyapunov exponent was found to be zero for this input speed as seen in Figure 3(b), indicating that the resulting motion is quasi-periodic.

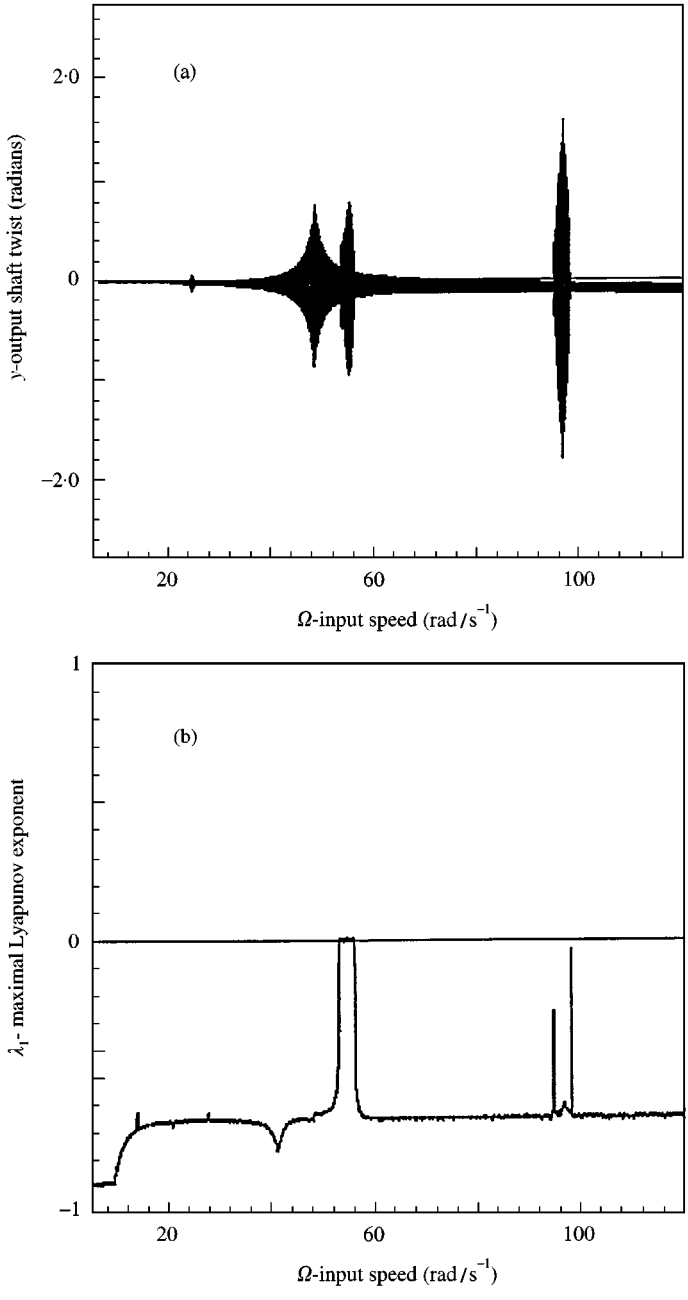

Figure 5. Variation of (a) extreme values of steady state twist, (b) maximal Lyapunov exponent: $\theta = 20^\circ$ and ω range of 5–120 rad/s.

The Hooke's joint angle θ is then decreased to 20°, and a diagram showing the variation of the extreme values of the steady state twist for input speeds from 5 to 120 rad/s is obtained as shown in Figure 5(a). It may be seen that the amplitude of output vibration is lower when compared to the case shown in Figure 3(a) and a number of instability regions have disappeared due to the presence of damping in the system. In fact, for the lower Hooke's joint angle, noticeable parametric instability is only associated with the

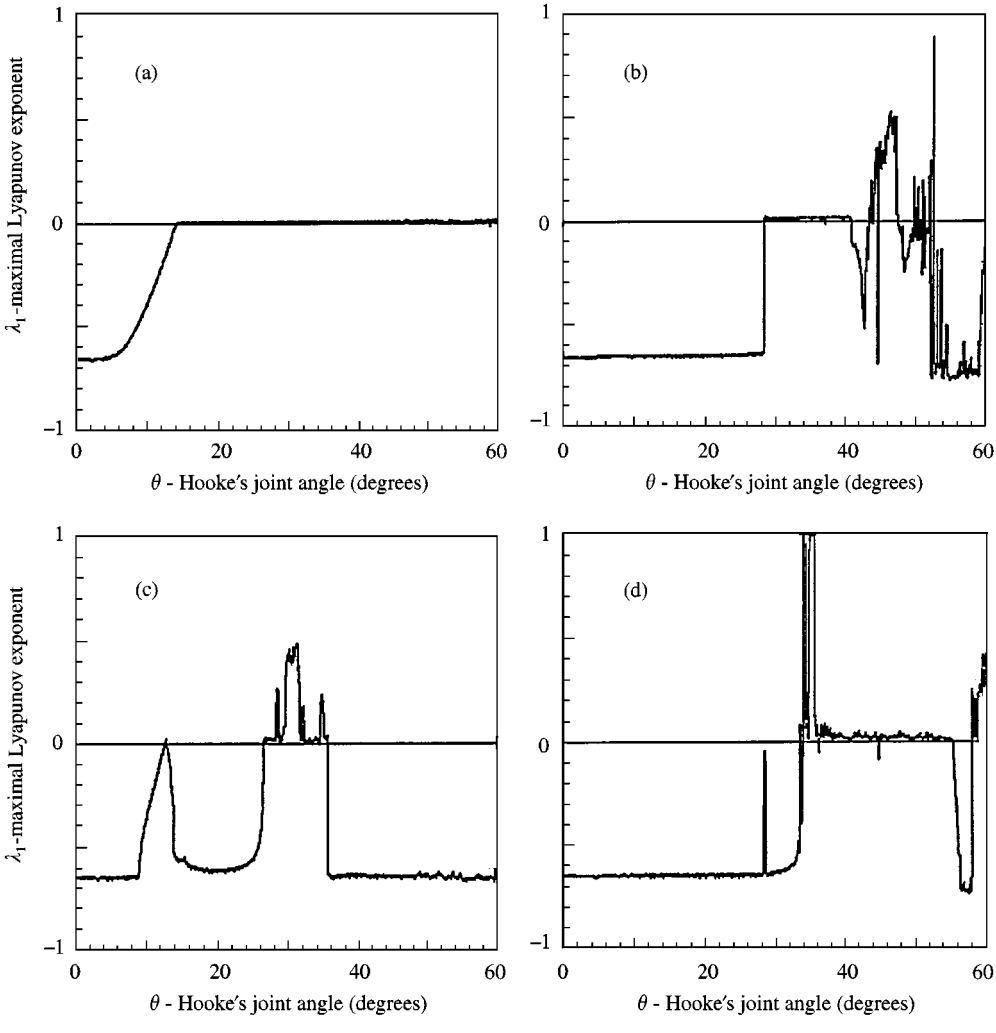

Figure 6. Variation of maximal Lyapunov exponent for θ range of 0–40°. (a) $\Omega = 55$ rad/s; (b) $\Omega = 62$ rad/s; (c) $\Omega = 97$ rad/s; (d) Ω of 100 rad/s.

combination and higher order sub-harmonic resonance cases. The diagram of maximum Lyapunov exponents for the same parameters shown in Figure 5(b) also indicates the same instability regions associated with sudden increases in the value of the maximum exponent. Comparison between the results depicted in Figures 3(b) and 5(b) indicates that the magnitudes of the maximum Lyapunov exponents are also dependent on the Hooke's joint angle. It may also be noted that no chaotic motion is present for a joint angle of 20°, indicating that the onset of chaotic motion is brought about through increased Hooke's joint angle.

5.2.2. *Case II*: *Predictions for Hooke's joint angle variation*

Figure 6(a) shows a diagram of maximum Lyapunov exponents for Hooke's joint driven system. For this case, the input speed Ω remained constant at 55 rad/s, close to the primary combination resonance frequency $(\omega_1 + \omega_2)/2$ and the Hooke's joint angle is varied from

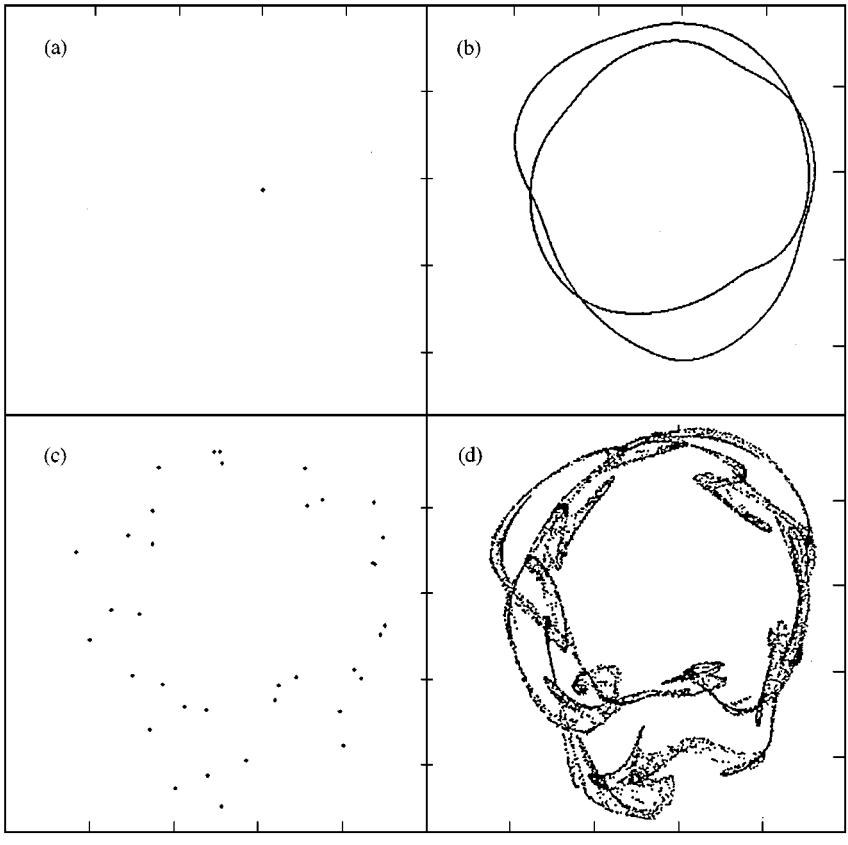

Figure 7. Poincare map history for $\omega = 62$ rad/s. (a) $\theta = 20°$; (b) $\theta = 30°$; (c) $\theta = 42°$; (d) $\theta = 45°$.

0 to 60°. From the diagram it is evident that for Hooke's joint angles less than 14°, instabilities due to combination resonance are not excited. As the Hooke's joint angle increases to 14° it is seen that the largest Lyapunov exponent increases towards zero but is still negative indicating less stability and that the motion is still periodic. It is found that the transient time to stable period-1 motion when Hooke's joint angle ranges from 0 to 4° increases with a maximum Lyapunov exponent. The maximum Lyapunov exponent is 0 throughout the Hooke's joint angle range of 14–60°, indicating quasi-periodic motion.

Figure 6(b) shows a diagram of maximum Lyapunov exponents for a constant input frequency Ω of 62 rad/s. In this case quasi-periodic motion occurs at a Hooke's joint angle of 28·5° and continues for all values up to 41° as indicated by the zero maximum Lyapunov exponent. For the interval of θ in the range of 41–43° the largest Lyapunov exponent becomes negative again indicating periodic motion. For Hooke's joint angles greater than 43°, the maximum Lyapunov exponent becomes positive indicating chaotic motion. This phenomenon persists until 47°, after which there are many intervals of periodic as well as chaotic motion until at 53° when the system settles to periodic motion again. This sequence of stable to quasi-periodic to periodic to chaotic motion is a typical example of the quasi-periodic route to chaos and has been documented by many other authors [10]. Figures 6(c) and 6(d) also depict similar bifurcation diagrams as Figure 6(b), also illustrating quasi-periodic routes to chaotic motion for constant input frequencies Ω of 97 and 100 rad/s.

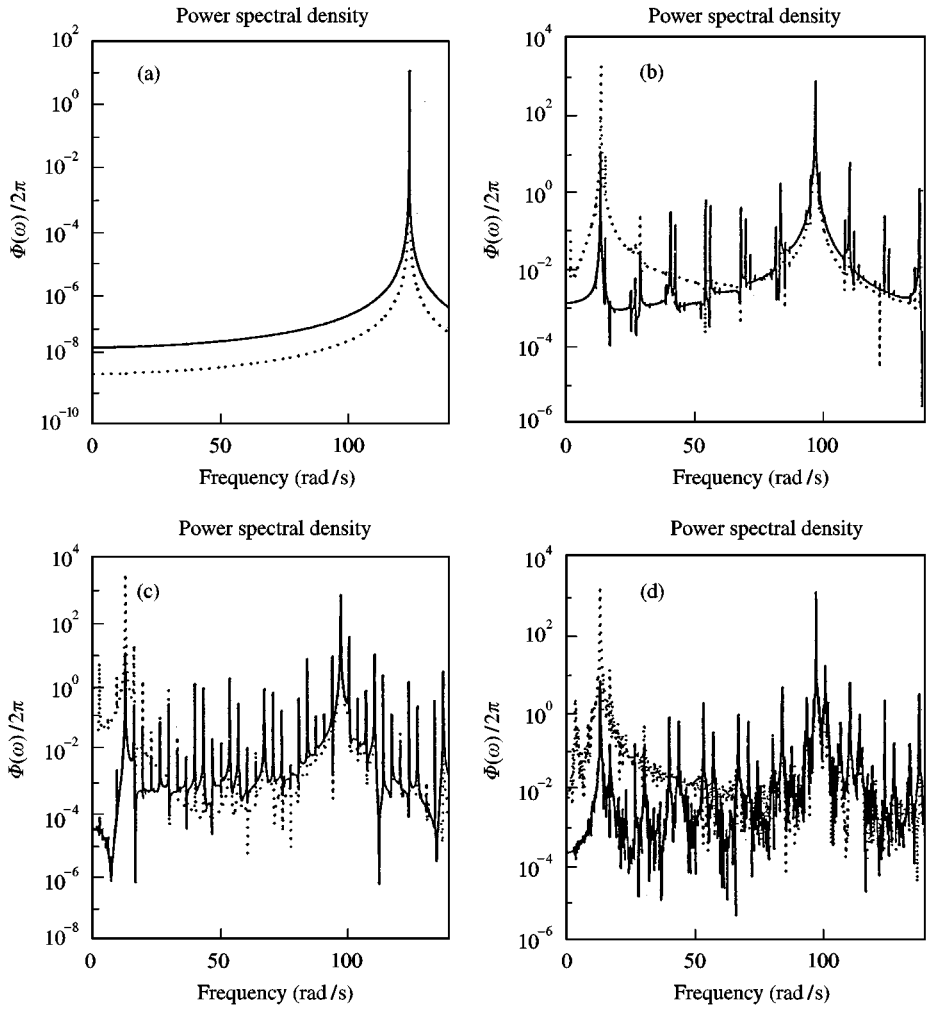

Figure 8. Power spectral density for $\omega = 62$ rad/s. (a) $\theta = 20°$; (b) $\theta = 30°$; (c) $\theta = 42°$; (d) $\theta = 45°$

Figure 7 shows a series of Poincare map diagrams of state variables y versus $\mathrm{d}y/\mathrm{d}t$ for simulations at a constant input frequency of 62 rad/s but for four different Hooke's joint angles while Figure 8 shows the frequency power spectra of the same cases. As illustrated in the maximal Lyapunov exponent diagram of Figure 5(b), for the Hooke's angle of 20° and an input frequency of 62 rad/s the system behaves in a stable manner. Figure 7(a) indicates that this motion is a period-1 stable limit cycle and the output frequency is equal to the Hooke's joint excitation frequency $2\Omega = 124$ rad/s as evident in Figure 8(a). Figure 7(b) reveals the quasi-periodic attractor on the Poincare map indicated by the closed curve for a Hooke's joint angle of 30°. This motion is identified in the power spectrum of Figure 8(b) by two distinct peaks and their multiples. The Lyapunov spectrum for these parameters was calculated to be [0·0 — 0·826 — 0·826 — 1·444]. At a Hooke's joint angle of 42° the periodic motion found in the Lyapunov diagram of Figure 5(b) is seen to be period-37 in the Poincare map of Figure 7(c). The power frequency spectrum of Figure 8(c) also indicates this through the finite and commensurate frequencies displayed. Finally, at a Hooke's angle of 45°, possible chaotic motion is indicated in Figure 7(d) by the infinite set of highly

organized points known as a strange attractor. The spectrum of Lyapunov exponents was calculated in this case to be [0·308 0 − 0·282 − 1·278 − 1·844], the positive value indicating possible chaotic motion. The power spectral density of Figure 8(d) depicts this also with a broad spectrum of frequencies. It may also be observed that the prediction of chaotic motion at this angle is not completely conclusive since the largest Lyapunov exponent is only slightly greater than zero and also the Poincare map appears to be well defined. Simulations were performed at other speeds when more conclusive evidence of choatic motion was observed via these indicators. However, the speed used in the simulation presented was chosen primarily for clearly demonstrating the transition through non-linear phenomena.

6. CONCLUSIONS

Non-linear vibration in a driveline which incorporates a Hooke's joint has been studied via an asymptotic method as well as numerical simulation. In particular, torsional vibration due to a fluctuating angular velocity ratio across the joint has been found to occur for particular input shaft speeds and for sufficiently large Hooke's joint angles. Linear analysis was used for predicting the onset of parametric instabilities using the method of averaging. Numerical simulations of the full non-linear equations of motion have shown the existence of parametric resonance as well as quasi-periodic and chaotic motion. It has been shown for increasing angle of misalignment in shafts, that onset of chaotic motion was characterized by the quasiperiodic route. From a practical point of view, the results obtained have shown that parametric instabilities of the subharmonic type close to the higher natural frequency as well as the combination type can be a problem for low Hooke's joint angles. It was also seen that very small variations in input shaft frequency as well as Hooke's joint angle could influence strongly the type of torsional vibrations of the system. This behaviour is a promising basis for the detailed examination of an experimental model of a driveline configuration incorporating a Hooke's joint.

REFERENCES

1. B. PORTER *The Journal of Mechanical Engineering Science* **3**, 324–329. A theoretical analysis of the torsional oscillation of a system incorporating a Hooke's joint.
2. B. PORTER and R. W. GREGORY 1963 *The Journal of Mechanical Engineering Science* **5**, 191–200. Non-linear torsional oscillation of system incorporating a Hooke's joint.
3. B. PORTER 1964 *Proceedings of the Royal Society of London Series A* **277**, 92–106. Non-linear torsional oscillation of a two-degree-of-freedom system incorporating a Hooke's joint.
4. S. F. ASOKANTHAN and HWANG 1995 *ASME Journal of Vibration and Acoustics*. Torsional instabilities in a system incorporating a Hooke's joint (accepted).
5. N. N. BOGOLIUBOV and Y. A. MITROPOLSKY 1961 *Asymptotic Methods in the Theory of Non-linear Oscillations*. New York: Gordon and Breach.
6. S. T. ARIARATNAM and S. F. ASOKANTHAN 1987 *Journal of Mechanisms, Transmissions and Automation in Design* (*ASME*) **109**, 412–418. Dynamic stability of chain drives.
7. S. F. ASOKANTHAN and S. T. ARIARATNAM 1994 *ASME Journal of Vibration and Acoustics*. **116**, 275–279. Flexural instabilities in axially moving bands.
8. H. E. NUSSE J. A. YORKE and E. KOSTELICH 1994 *Dynamics: An Interactive Program for IBM-Compatible PCs and for UNIX Computers* (*Computer File*). New York: Springer Verlag.
9. A. WOLF, J. B. SWIFT, H. L. SWINNEY and J. A. VASANO 1985 *Physica D* **16**, 285–317. Determining Lyapunov exponents from a time series.
10. R. C. HILBORN 1994 *Chaos and Nonlinear Dynamics: An Introduction for Scientists and Engineers*. New York: Oxford University Press.